EurJIC European Journal of Inorganic Chemistry
ChemPubSoc Europe
FULL PAPER

DOI:10.1002/ejic.201300184

A Robust Mn Catalyst for H_2O_2 Disproportionation in Aqueous Solution

CLUSTER ISSUE

Wei-Tsung Lee,[a] Song Xu,[a] Diane A. Dickie,[b] and Jeremy M. Smith*[a]

Keywords: Manganese / Reaction mechanisms / Peroxides / Homogeneous catalysis / Macrocycles

The pyridinophane complex $[Mn(Py_2N_2)(H_2O)_2]^{2+}$ catalyses the disproportionation of H_2O_2 in aqueous solution over a wide pH range. Kinetic investigations reveal an induction period, which is proposed to involve the formation of a hydroperoxo intermediate, as well as evidence for catalyst self-inhibition. A catalytic cycle involving mononuclear intermediates has been proposed. Spectroscopic investigations under turnover conditions are consistent with this proposal and show that the resting state of the catalyst is a mononuclear Mn^{II} complex. The robustness of the catalyst is evidenced by its ability to achieve turnover numbers of 58000 in aqueous solution.

Introduction

Excess levels of reactive oxygen species (ROS) are implicated in a number of pathologies, such as tissue injury, inflammatory disorders, cardiovascular diseases, pulmonary diseases, and neurodegenerative diseases.[1] Hydrogen peroxide is one type of ROS that is formed by aerobic organisms through the partial reduction of O_2. In the presence of metal ions, H_2O_2 can be decomposed in Fenton-like reactions to provide the highly reactive hydroxyl radical, which readily oxidizes cellular macromolecules.

Cellular antioxidant defences are used to detoxify ROS by reducing them to water. In the case of H_2O_2, catalase enzymes catalyse the disproportionation of H_2O_2 to O_2 and H_2O:

$$2\ H_2O_2 \rightarrow O_2 + 2\ H_2O$$

There are two catalase families. The more common heme-containing catalases contain an iron(III) protoporphyrin IX prosthetic group,[2] whereas the Mn-containing catalases (MnCAT) have an active site with two Mn ions bridged by carboxylato and single-atom ligands (likely water or hydroxide).[3,4]

The structure and reactivity of MnCAT has motivated the synthesis of many functional model complexes for the catalysis of H_2O_2 disproportionation.[5] Whereas most of these complexes are structurally related to MnCAT in that they are either prepared as or assemble into Mn_2 dimers under catalytic conditions, a smaller class of MnCAT mimics appears to remain monomeric during catalysis. Most of these catalysts are only active in organic or mixed aqueous–organic solvents at a relatively high pH. Despite these limitations, a number of Mn complexes have been investigated as low-molecular-weight catalytic antioxidants for treating overt inflammation associated with excess H_2O_2,[6] most notably, (porphyrin)Mn^{III}[7] and (salen)Mn^{III}[8] complexes.

We report a new catalyst for H_2O_2 disproportionation, namely, the (pyridinophane)Mn^{II} complex $[Mn(Py_2N_2)(H_2O)_2]^{2+}$ {Figure 1, Py_2N_2 = *N*,*N*′-dimethyl-2,11-diaza[3,3](2,6)pyridinophane}. This catalyst is remarkably robust, operating over a wide pH range in aqueous solution. Mechanistic studies provide evidence for a reaction mechanism that involves a monomeric catalyst. Although the rate of H_2O_2 disproportionation is intermediate, the catalyst is long-lived, achieving turnover numbers of 58000.

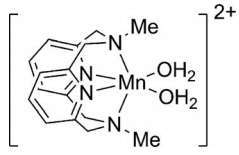

Figure 1. $[Mn(Py_2N_2)(H_2O)]^{2+}$.

Results and Discussion

The reaction of *N*,*N*′-dimethyl-2,11-diaza[3,3](2,6)pyridinophane with $MnBr_2$ leads to the formation of the (macrocycle)Mn^{II} complex $Mn(Py_2N_2)Br_2$ in high yield. The anal-

[a] Department of Chemistry and Biochemistry, New Mexico State University,
Las Cruces, NM 88003, USA
Fax: +1-575-646-2649
E-mail: jesmith@nmsu.edu
Homepage: http://www.chemistry.nmsu.edu/Faculty/SMITHJEREMY.htm
[b] Department of Chemistry and Chemical Biology, The University of New Mexico,
Albuquerque, NM 87131, USA
Supporting information for this article is available on the WWW under http://dx.doi.org/10.1002/ejic.201300184.

ogous chloride complex $Mn(Py_2N_2)Cl_2$ has been previously reported.[9,10] The conductivity Λ_M of the complex in aqueous solution (Λ_M = 268 $\Omega^{-1}cm^2mol^{-1}$) is consistent with the presence of three ions, and therefore the complex is fully aquated as $[Mn(Py_2N_2)(H_2O)_2]^{2+}$ at pH = 7 (Figure 1). The magnetic susceptibility of $[Mn(Py_2N_2)(H_2O)_2]^{2+}$, determined by the Evans method, is χ_M = 5.91(3) μ_B, which is consistent with high-spin Mn^{II} (S = 5/2). The EPR spectrum is also consistent with Mn^{II}, resembling the spectra of certain non-heme Mn^{II} enzymes.[11,12] The complex is slightly air-sensitive, and its aqueous solutions develop a yellow colour over the course of several days.

Hydrogen peroxide is catalytically disproportionated by $[Mn(Py_2N_2)(H_2O)_2]^{2+}$. Disproportionation is observed in aqueous solution over a wide pH range (pH = 2–8.5). In contrast, most other Mn catalysts for H_2O_2 disproportionation are only active at high pH values.[5] At higher pH values, no difference to the background H_2O_2 decomposition is observed. Interestingly, the catalyst is remarkably long-lived, achieving a turnover number of 58000 when the initial pH is 4.3. The robustness of $[Mn(Py_2N_2)(H_2O)_2]^{2+}$ is noteworthy, as the complex achieves very high turnover numbers and operates over a relatively wide pH range, which includes very acidic conditions, under which most other catalase mimics are inactive. Given the relative rarity of mononuclear Mn catalysts for H_2O_2 disproportionation, particularly in aqueous solution, as well as the robustness of this particular catalyst, we have undertaken investigations towards understanding the catalytic mechanism.

Attempts to determine the initial rates of O_2 evolution at relatively low H_2O_2 concentrations (<1 mM) with a Clark-type electrode were plagued by difficulties in reproducibility. However, at very high H_2O_2 concentrations (3.1–6.1 M) a reproducible kinetic behaviour was observed. Additionally, because decreased reaction rates were observed in buffer solutions, all kinetic experiments were conducted in unbuffered aqueous solutions.

The initial rates of H_2O_2 decomposition, as determined by volumetric measurements of the evolved O_2, were proportional to $[H_2O_2]$ with no evidence of saturation kinetics.[11] In contrast, the dependence of the initial rate constants on the catalyst concentration reveals saturation kinetics (Figure 2a). A double-reciprocal plot of this data is linear (Figure 2b), and thus the kinetic behaviour fits the following equation:

$$k_{obs} = \frac{kK[Mn]}{1 + K[Mn]}$$

with k = 1.8(5) and K = 0.01(2).

This saturation behaviour suggests that catalyst self-inhibition occurs at higher concentrations, for example, by the formation of catalytically inactive dimers.

At $[Mn(Py_2N_2)(H_2O)_2]^{2+}$ concentrations below the saturation limit, the second-order rate constant for the H_2O_2 disproportionation k = 0.176(7) $M^{-1}s^{-1}$ is smaller than those of many other reported catalysts that follow second-order kinetics (Table 1),[13] although it is significantly faster than Mn^{III}(salen)Cl (EUK-134), a catalase mimic that has been investigated as a catalytic antioxidant.[8,14] It should be noted that a range of conditions have been used for these measurements. An H/D kinetic isotope effect (KIE) of 0.8 is observed for the disproportionation of isotopically enriched hydrogen peroxide in a D_2O/H_2O solution.[15] An Eyring

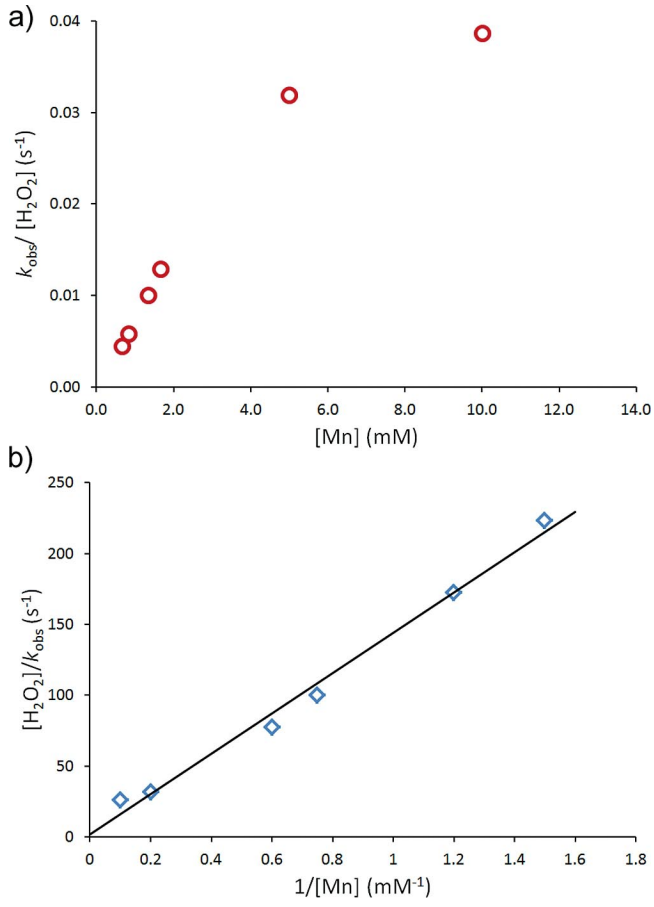

Figure 2. (a) Dependence of the initial rate of H_2O_2 decomposition on the concentration of $[Mn(Py_2N_2)(H_2O)_2]^{2+}$ catalyst. Initial $[H_2O_2]$ = 3.1 M. (b) Doubly reciprocal plot of the same data.

Table 1. Monometallic Mn catalysts for H_2O_2 disproportionation that exhibit second-order kinetics.

Precatalyst[a]	k [$M^{-1}s^{-1}$]	Solvent	Ref.
Mn^{II}(bimindH)Cl_2	4.12	EtCN	[17]
Mn^{II}(indH)Cl_2	1.55	MeCN	[18]
Mn^{II}(pbmpa)Cl	0.478	H_2O[b]	[19]
Mn^{II}(mpbmpa)Cl_2	0.636	H_2O[b]	[19]
Mn^{II}{(3-OMe)salen}	0.00417	DMF/H_2O	[20]
Mn^{II}{(3-OMe)salen}(imidazole)	0.00794	DMF/H_2O	[20]
Mn^{III}(salen)Cl	4.97×10^{-6}	H_2O[c]	[8]
$[Mn^{III}\{(C_6F_5)_3(SO_3)_2\}(corrole)]^{2-}$	5.6	H_2O[d]	[21]
$[Mn^{II}(Py_2N_2)(H_2O)_2]^{2+}$	0.18	H_2O[e]	this work

[a] bimindH = 1,3-bis(2′-benzimidazolylimino)isoindoline; indH = 1,3-bis(2′-pyridylimino)isoindoline; pbmpa = 3-[bis(2-pyridylmethyl)amino]propanoate; mpbmpa = methyl 3-[bis(2-pyridylmethyl)amino]propanoate (see the Supporting Information for structures of the ligands). [b] Maximum rate observed at pH = 11, phosphate buffer. [c] pH = 8.1. [d] pH = 9.5. [e] Initial pH = 5.5, [Mn] = 0.33 mM, unbuffered.

analysis of the temperature-dependent rate constants (T = 25–44 °C) gives the activation parameters $\Delta H^{\ddagger}$ = +13.5(8) kcal mol^{-1} and $\Delta S^{\ddagger}$ = +25(2) J mol^{-1} K^{-1}. The large positive value of $\Delta S^{\ddagger}$ is notable and is similar to the entropy of activation for dissociative ligand-substitution reactions.[16]

An induction period for the O_2 formation was observed during the kinetic measurements. This induction period shows no H/D isotope effect and is concomitant with a decrease in the solution pH (Figure 3) as well as with the growth of a band at approximately 390 nm in the UV/Vis spectrum.[11] Whereas this band decays after the induction period, no further change in the solution pH is observed. These observations suggest that the induction period is associated with a deprotonation step. The magnitude of the pH change (ca. 1.3 pH units) is an order of magnitude smaller than the initial concentration of $[Mn(Py_2N_2)(H_2O)_2]^{2+}$ (0.67 mM), and it is insufficient to account for the complete deprotonation of all the Mn complex molecules in solution.

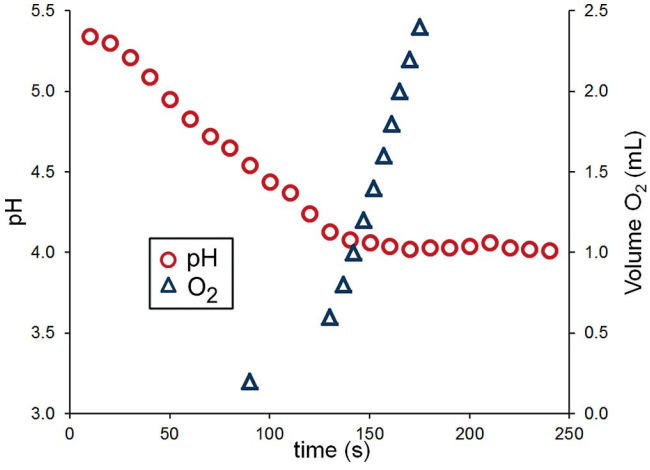

Figure 3. Change of pH and induction period for the O_2 formation. Initial conditions: [Mn] = 0.67 mM, [H_2O_2] = 3.1 M, aqueous solution, 298 K.

One possible pathway of O_2 formation involves the homolysis of the O–O bond in H_2O_2, which leads to hydroxyl radical formation. To test this possibility, we investigated the bleaching of methylene blue in the presence of H_2O_2 and $[Mn(Py_2N_2)(H_2O)_2]^{2+}$.[22] Under pseudo-first-order conditions, the initial rate of bleaching k_{obs} was determined by UV/Vis spectroscopy [$k_{obs} = 1.05(5) \times 10^{-3}$ s^{-1}]. Control experiments established that both the catalyst and H_2O_2 are required to bleach methylene blue. However, the rate of bleaching is the same in the presence of excess *t*BuOH, which reacts as an OH$^{\cdot}$ scavenger [$k_{obs} = 1.01(2) \times 10^{-3}$ s^{-1}]. Thus, O–O bond homolysis is unlikely to be significant in the reaction mechanism, and OH$^{\cdot}$ does not play an important role in the methylene blue bleaching. As with H_2O_2 disproportionation, there is also an induction period for the bleaching of methylene blue. This induction period is also associated with the growth of a band at 390 nm in the UV/Vis spectrum, which suggests that H_2O_2 disproportionation and methylene blue bleaching involve common intermediates.

We have also tested the possibility of superoxide formation during catalysis by using red-CLA.[23,24] However, there is no change in the fluorescence spectrum of the dye under catalytic conditions, and thus the formation of free superoxide during catalysis is also unlikely.

To obtain spectroscopic information about the nature of the catalytic intermediates, the EPR spectrum of $[Mn(Py_2N_2)(H_2O)_2]^{2+}$ was measured in the presence of excess H_2O_2 (Figure 4). Interestingly, the EPR spectrum, which is different from that of the starting complex, reveals a single Mn^{II} species with no evidence of significant amounts of Mn^{III} or Mn^{IV}. Moreover, because the integrated signals of $[Mn(Py_2N_2)(H_2O)_2]^{2+}$ before and after the addition of H_2O_2 are the same, the formation of significant amounts of EPR-silent species is unlikely. Thus, the spectroscopic data strongly suggest that the catalyst resting state is a mononuclear Mn^{II} species that is not $[Mn(Py_2N_2)(H_2O)_2]^{2+}$.

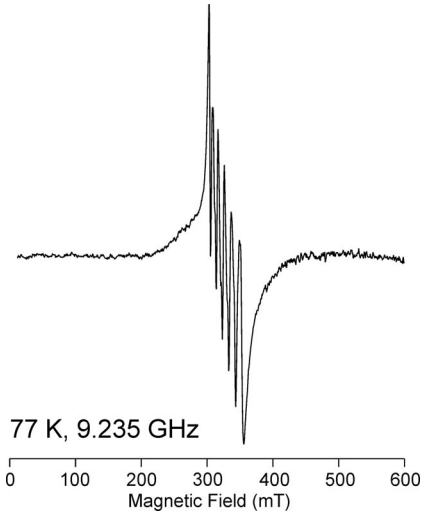

Figure 4. EPR spectrum of $[Mn(Py_2N_2)(H_2O)_2]^{2+}$ in the presence of excess H_2O_2. Initial conditions: [Mn] = 4 μM, [H_2O_2] = 20 mM.

A mechanism consistent with the experimental data is presented in Scheme 1. Entry into the catalytic cycle involves the substitution of an aqua ligand by H_2O_2 and a subsequent deprotonation, which yields the (aqua)(hydroperoxido)Mn^{II} complex $[Mn(Py_2N_2)(H_2O)(O_2H)]^{2+}$. Because H_2O_2 is a poor ligand,[25] the substitution step is expected to be rate-determining for the catalyst induction, which is consistent with the lack of an H/D isotope effect. The equilibrium for this step is likely to favour the reactants. Therefore, we propose that the slow formation of $[Mn(Py_2N_2)(H_2O)(O_2H)]^{+}$ accounts for the observed induction period. We note that it is also possible that H_2O_2 binds in a bidentate fashion to provide $[Mn(Py_2N_2)(\kappa^2\text{-}O_2H)]^{+}$. However, for the sake of clarity, only species, in which H_2O_2 is monodentate, will be discussed.

An aqua-ligand-assisted intramolecular O–O bond heterolysis in the hydroperoxido complex (with loss of water) is

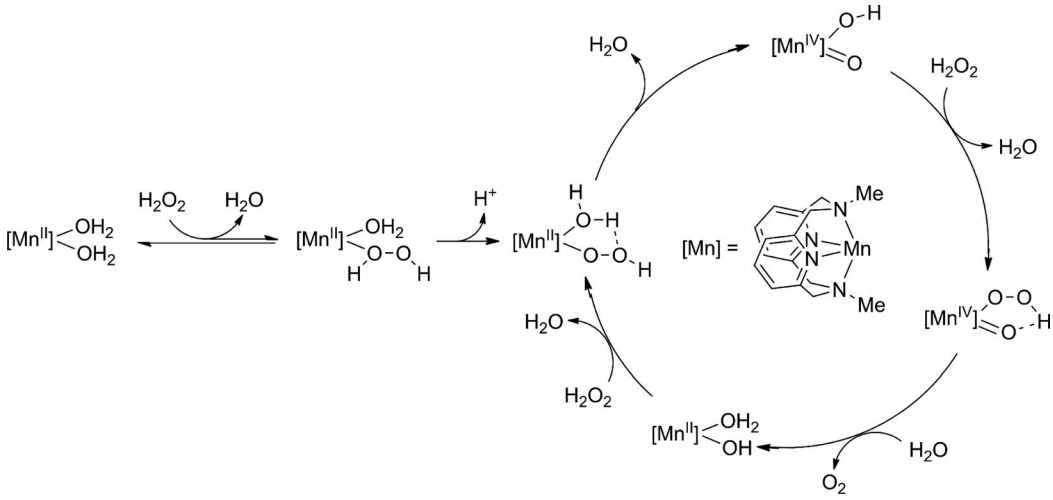

Scheme 1. Proposed mechanism for the H_2O_2 disproportionation catalysed by $[Mn(Py_2N_2)(H_2O)_2]^{2+}$. Side reactions, such as catalyst self-inhibition, are not shown.

proposed to provide the (hydroxido)(oxido)Mn^{IV} intermediate $[Mn(Py_2N_2)(O)(OH)]^+$, similar to mechanistic proposals for non-heme (hydroperoxido)iron complexes.[26] The alternate possibility of O–O bond homolysis can be discounted, as there is little evidence for hydroxyl radical formation. Heterolysis of the O–O bond is often observed in (hydroperoxido)manganese complexes.[27] The loss-of-coordinated-water step is also consistent with the large positive value of $\Delta S^{\ddagger}$. We also note that a (hydroxido)(oxido)Mn^{IV} complex supported by a related macrocyclic ligand, $[Mn(Me_2EBC)(O)(OH)]^+$ (Me_2EBC = 4,11-dimethyl-1,4,8,11-tetraazabicyclo[6.6.2]hexadecane) has been characterized.[28,29]

The reaction of $[Mn(Py_2N_2)(O)(OH)]^+$ with a second molecule of H_2O_2 provides the (hydroperoxido)(oxido)-Mn^{IV} species $[Mn(Py_2N_2)(O)(OOH)]^+$.[30] It is likely that this species is the active oxidant in the methylene blue bleaching by $[Mn(Py_2N_2)(H_2O)_2]^{2+}$ and H_2O_2.[31] The lowest-energy conformation of $[Mn(Py_2N_2)(O)(OOH)]^+$ is expected to have an intramolecular hydrogen bond between the hydroperoxido and the oxido ligand.[32] This conformation facilitates intramolecular proton transfer, which leads to the reductive elimination of O_2 and the formation of the (aqua)(hydroxido)Mn^{II} complex $[Mn(Py_2N_2)(OH)(OH_2)]^+$. An acid/base reaction between this species and H_2O_2 regenerates the (aqua)(hydroperoxido) species $[Mn(Py_2N_2)-(H_2O)(O_2H)]^{2+}$ along with H_2O.

The EPR spectrum recorded under turnover conditions is also consistent with this proposed mechanism and suggests that the (aqua)(hydroxido) complex $[Mn(Py_2N_2)-(H_2O)(O_2H)]^+$ is likely to be the resting state of the catalyst. On the basis of the Eyring analysis, the step leading to the cleavage of the O–O bond is expected to be the rate-determining step in the catalytic cycle. The observed catalyst self-inhibition may be due to the reversible formation of a dimer having an $[Mn(\mu\text{-}O)_2Mn]$ (or related) core. The irreversible formation of such dimers is expected to be unlikely on the basis of results observed for the similarly sized Me_2EDC ligand,[29] for which only monomeric oxido complexes have been observed.

As noted above, we have observed that the decrease in pH associated with the induction period is insufficient to account for the deprotonation of all the $[Mn(Py_2N_2)-(H_2O)_2]^{2+}$ molecules in solution. One possible explanation is that the hydroxido ligand in $[Mn(Py_2N_2)(OH)(OH_2)]^+$ is reprotonated by the previously released H^+ ions to regenerate the starting bis(aqua)Mn^{II} complex $[Mn(Py_2N_2)-(H_2O)_2]^{2+}$. The formation of this dormant complex would account for the substoichiometric decrease in the solution pH during the induction period. Alternatively, it is possible that not all metal complex molecules enter the catalytic cycle.

It is interesting to contrast the reactivity of the pyridinophane complex $[Mn(Py_2N_2)(H_2O)_2]^{2+}$ towards H_2O_2 with that of Mn complexes supported by related ligands. The strapped cyclam ligand Me_2EBC provides a coordination environment similar to that of Py_2N_2, most notably creating *cis* coordination sites for substrate binding, but it binds through different donor groups. Although H_2O_2 disproportionation by $[Mn(Me_2EBC)(H_2O)_2]^{2+}$ was noted, the complex was ultimately oxidized by H_2O_2 to afford purple $[Mn^{IV}(Me_2EBC)(OH)_2]^{2+}$,[29] which is in contrast to our observations for $[Mn(Py_2N_2)(H_2O)_2]^{2+}$. It is likely that this difference is due to the ability of the Me_2EBC ligand to better stabilize higher oxidation states, which is reflected by comparative electrochemical data.[33,34]

Although the tetradentate open-chain ligand bipicen [bispicen = *N*,*N*′-dimethyl-*N*,*N*′-bis(2-pyridylmethyl)ethane-1,2-diamine] contains the same donor groups as Py_2N_2, the reaction of Mn^{II}(bispicen)Cl_2 with stoichiometric amounts of H_2O_2 affords the corresponding dimer $[Mn_2(bispicen)_2(\mu\text{-}O)_2]^{3+}$.[35] This is likely a result of the ligand being insufficiently bulky to thwart the formation of the bis(μ-oxido) dimer. Similarly, the formation of [Mn(μ-

$O)_2Mn]$ dimers from the reaction of (cyclam)Mn^{II}[36] and (cyclen)Mn^{II}[37] complexes is also related to the reduced steric bulk of these macrocycles.

Conclusions

The Mn^{II} complex $[Mn(Py_2N_2)(H_2O)_2]^{2+}$ is a precursor to a H_2O_2 disproportionation catalyst. The catalyst is robust, being active over a wide pH range and achieving very high turnover numbers. On the basis of mechanistic and spectroscopic investigations, we have proposed a catalytic cycle that involves only monomeric intermediates. The structural features of the pyridinophane ligand are believed to be critical to the catalytic reactivity, namely, its ability to stabilize monomeric species with vacant *cis* coordination sites.

Experimental Section

General Remarks: All anaerobic manipulations were performed under nitrogen by using standard Schlenk techniques or in an M. Braun Labmaster glovebox. Glassware was dried at 150 °C overnight. Diethyl ether, tetrahydrofuran, DMF, and acetonitrile were purified with a Glass Contour solvent purification system. Deionized water was used for all kinetic and volumetric measurements. The compounds 2,6-bis(chloromethyl)pyridine, tosylamide monosodium salt (TsNHNa), and 2,11-diaza[3,3](2,6)pyridinophane were prepared according to literature procedures.[38,39] The concentration of H_2O_2 was determined by a redox titration with potassium permanganate. All other reagents were purchased from commercial vendors and used as received. ^1H NMR spectroscopic data were recorded with a Varian Unity 400 spectrometer (400 MHz) at 22 °C. The stock solution of red-CLA (250 μM) was prepared by dissolving red-CLA (1 mg) in a H_2O/MeOH mixture (1:1, v/v; 4.2 mL). Photoluminescence spectra were recorded with a CARY Eclipse fluorescence spectrophotometer. Solution magnetic susceptibilities were determined by using the Evans method.[40] UV/Vis spectra were recorded with a CARY 100 Bio UV/Vis spectrophotometer. The conductivity of the complex in H_2O at 25 °C was measured with a Radiometer CDM 83. All pH measurements were acquired with an Orion Star A111 pH meter by using a glass electrode (Orion 9157BNMD). High-resolution mass spectrometry was conducted through positive electrospray ionization with a Bruker 12 Tesla APEX-Qe FTICR-MS with an Apollo II ion source at the mass spectrometry facility at Old Dominion University, Norfolk, VA. X-band (ca. 9–9.5 GHz) EPR spectra were recorded with a modified Varian E-9 spectrometer by using DPPH (2,2-diphenyl-1-picrylhydrazyl) as an external standard.

Synthesis of *N,N′*-Ditosyl-2,11-diaza[3,3](2,6)pyridinophane: This compound was prepared according to published procedures with slight modifications.[39] A solution of 2,6-bis(chloromethyl)pyridine (1.8 g,10.2 mmol) in *N,N*-dimethylformamide (20 mL) was added dropwise to a stirred slurry of TsNHNa (2.0 g, 10.4 mmol) in *N,N*-dimethylformamide (200 mL) at 80 °C over a period of 1 h. Solid TsNHNa (2.0 g, 10.4 mmol) was added all at once, and the reaction mixture was stirred at 80 °C for 4 h. The volatiles were removed under reduced pressure to obtain a sticky solid, which was washed with water (50 mL) followed by methanol (20 mL) and ethanol (20 mL). The remaining white residue was continuously extracted with acetone (100 mL) in a Soxhlet apparatus overnight. The extract was concentrated to dryness to afford the desired product. Yield: 1.1 g (39%). The spectral properties are identical to those reported in the literature.

Synthesis of *N,N′*-Dimethyl-2,11-diaza[3,3](2,6)pyridinophane (Py_2N_2): 2,11-Diaza[3,3](2,6)pyridinophane (0.25 g, 1.0 mmol), 37% formaldehyde (4.4 g, 4.0 mL, 54.3 mmol), and formic acid (3.1 g, 2.5 mL, 67.3 mmol) were heated at reflux for 24 h. The reaction mixture was basified with 2 N NaOH, extracted with dichloromethane (2 × 50 mL), and the extracts were dried with sodium sulfate. Removal of the volatiles under reduced pressure furnished an off-white solid, which was purified by recrystallization from *n*-hexane. Yield: 0.19 g (71%). The spectral properties are identical to those reported in the literature.[39]

Synthesis of $Mn(Py_2N_2)Br_2$: A slurry of $MnBr_2$ (107 mg, 0.5 mmol) in THF (3 mL) was mixed with Py_2N_2 (134 mg, 0.5 mmol) in THF (2 mL) and stirred at ambient temperature under N_2 for 3 h. The reaction mixture was filtered through a sintered glass filter and washed with tetrahydrofuran (5 mL) to afford a solid. The product was purified by slow diffusion of diethyl ether into an acetonitrile solution of the complex at –30 °C. A yellow solid was obtained. Yield: 210 mg (87%). HRMS (ESI): calcd. for $C_{16}H_{20}BrMnN_4$ $[M - Br]^+$ 402.0252; found 402.0243. μ_{eff} = 5.91(3) μ_B. $\Lambda_M(H_2O)$ = 268 $\Omega^{-1}\,cm^2\,mol^{-1}$.

Synthesis of $[Mn(Py_2N_2)(NCMe)_2](PF_6)_2$: A solution of $TlPF_6$ (210 mg, 0.6 mmol) in acetonitrile (2 mL) was added to a stirred solution of $Mn(Py_2N_2)Br_2$ (145 mg, 0.3 mmol) in acetonitrile (3 mL) under N_2. The reaction mixture was stirred at ambient temperature for 3 h. After filtration through Celite, the removal of volatiles furnished a white solid. Crystals suitable for X-ray diffraction analysis were grown by slow diffusion of diethyl ether into an acetonitrile solution of the complex at –30 °C. Yield: 0.16 g (77%).

Kinetics Measurements: Oxygen evolution studies were carried out volumetrically under pseudo-first-order conditions. The reactions were performed in a sealed Erlenmeyer flask (25 mL) immersed in a water bath thermally equilibrated at 25 °C and equipped with a stirring bar and a gas-delivery side tube connected to an inverted burette filled with water. The flask was charged with $Mn(Py_2N_2)Br_2$ (in 1 mL H_2O, 1–5 μmol) and water (0–1 mL). H_2O_2 (1–2 mL, 9.2–18.4 mmol) was added with a syringe, and the reaction mixture was stirred vigorously at a constant stirring rate (300 rpm). The stopwatch was started right after the addition of H_2O_2. The initial-rate method was used to determine the rate constants. Each rate constant reported represents the average value of duplicate or triplicate determinations. Variable-temperature kinetic experiments were carried out over the temperature range 25–44 °C.

Reaction of Mn Complexes with H_2O_2 and Quantification of O_2 Evolution: The reactions were performed in a sealed Erlenmeyer flask (50 mL) immersed in a water bath at 25 °C and equipped with a stirring bar and a gas-delivery side tube connected to an inverted graduated cylinder filled with water. The flask was charged with $Mn(Py_2N_2)Br_2$ (in 0.5 mL H_2O, 1.5 μmol) and water (0.5 mL). H_2O_2 (10 mL, 9.7 mmol) was added with a syringe, and the reaction mixture was stirred vigorously. The stopwatch was started right after the addition of H_2O_2. The amount of evolved dioxygen was determined volumetrically, and the yield of O_2 was calculated by using the ideal gas law and by accounting for the reduced atmospheric pressure in Las Cruces. A turnover number of 58000 was calculated.

Kinetic Isotope Experiment: The experiment was performed in a sealed Erlenmeyer flask (10 mL) immersed in a water bath at 25 °C

and equipped with a stirring bar and a gas-delivery side tube connected to an inverted buret filled with water. The flask was charged with 9.2 M H_2O_2 (1 mL, 9.2 mmol) and D_2O (1.9 mL, 103 mmol). After aging for 1 h,[41] $Mn(Py_2N_2)Br_2$ (20 mM, 2.0 μmol) in D_2O (0.1 mL, 5 mmol) was added with a syringe, and the reaction mixture was stirred vigorously at a constant stirring rate (300 rpm). The stopwatch was started immediately after the addition, and the dioxygen amount was quantified volumetrically.

Methylene Blue Bleaching: A 1 cm cuvette was charged with methylene blue (in 1 mL H_2O, 0.05 μmol) and H_2O_2 (1 mL, 92 mmol). An aqueous solution of $Mn(Py_2N_2)Br_2$ (in 1 mL H_2O, 1 μM) was added, and the reaction mixture was stirred vigorously for 2 s. The decay of the characteristic absorbance of methylene blue at 665 nm was monitored by UV/Vis spectroscopy.

Superoxide Detection: A 1 cm cuvette was charged with $Mn(Py_2N_2)Br_2$ (in 1.44 mL H_2O, 1.44 μmol) and H_2O_2 (1.44 mL, 132 μmol). A stock solution of red-CLA (0.12 mL, 0.03 μmol) was added, and the reaction mixture was stirred vigorously for 2 s. The emission at 610 nm was measured with a fluorescence spectrophotometer. There was no difference between the fluorescence spectra recorded under catalytic conditions and similar control experiments for solutions of $Mn(Py_2N_2)Br_2$, H_2O_2, and only red-CLA.

X-ray Crystallography: For the X-ray crystallographic analysis, a colourless block-like specimen of $C_{20}H_{26}F_{12}MnN_6P_2$ (approximate dimensions 0.26 mm × 0.29 mm × 0.42 mm) was cut from a larger crystal, coated with Paratone oil, and mounted on a CryoLoop that had been previously attached to a metal pin by using epoxy. The X-ray intensity data were measured with an APEX II CCD system equipped with a graphite monochromator and a Mo-K_α sealed tube (λ = 0.71073 Å). The frames were integrated with the Bruker SAINT software package by using a narrow-frame algorithm. The integration of the data using a monoclinic unit cell yielded a total of 42198 reflections to a maximum θ angle of 28.28° (0.75 Å resolution), of which 7289 were independent (average redundancy 5.789, completeness = 99.7%, R_{int} = 3.27%, R_{sig} = 2.30%), and 5972 (81.93%) were larger than $2\sigma(F^2)$. The final cell constants of a = 9.3168(9) Å, b = 16.8827(16) Å, c = 20.5176(18) Å, β = 114.245(5)°, and V = 2942.6(5) Å^3 are based on the refinement of the XYZ centroids of reflections above $20\sigma(I)$. The calculated minimum and maximum transmission coefficients (based on the crystal size) are 0.7703 and 0.8481, respectively. The structure was solved and refined by using the Bruker SHELXTL Software Package and by using the space group $P2_1/c$, with Z = 4 for the formula unit $C_{20}H_{26}F_{12}MnN_6P_2$. Non-hydrogen atoms were refined anisotropically. Hydrogen atoms were placed in geometrically calculated positions with $U_{iso} = 1.2U_{equiv}$ of the parent atom ($U_{iso} = 1.5U_{equiv}$ for methyl groups). The final anisotropic full-matrix least-squares refinement on F^2 with 374 variables converged at $R1$ = 3.98% for the observed data and at $wR2$ = 11.54% for all data. The goodness-of-fit was 1.046. The largest peak in the final difference electron density synthesis was 0.665 e$^-$Å^{-3}, and the largest hole was –0.516 e$^-$Å^{-3} with an RMS deviation of 0.068 e$^-$Å^{-3}. On the basis of the final model, the calculated density was 1.570 g cm^{-3}, and F(000) was 1404 e$^-$. CCDC-923209 contains the supplementary crystallographic data for this paper. These data can be obtained free of charge from The Cambridge Crystallographic Data Centre via www.ccdc.cam.ac.uk/data_request/cif.

Supporting Information (see footnote on the first page of this article): Structures of the ligands in Table 1, EPR spectrum of $[Mn(Py_2N_2)(H_2O)_2]^{2+}$, additional kinetic plots.

Acknowledgments

Financial support from Department of Energy – Basic Energy Sciences (DOE-BES) (DE-FG02-08ER15996) and American Chemical Society – Petroleum Research Foundation (ACS-PRF) (50971-ND3) is gratefully acknowledged. J. M. S. is a Dreyfus Teacher-Scholar. We thank Joshua Telser (Roosevelt University) for recording the EPR spectra and Michael D. Johnson (NMSU) for invaluable scientific assistance.

[1] a) V. Costa, P. Moradas-Ferreira, *Mol. Aspects Med.* **2001**, *22*, 217–246; b) D. S. Warner, H. Sheng, I. Batinić-Haberle, *J. Exp. Biol.* **2004**, *207*, 3221–3231; c) M. Valko, D. Leibfritz, J. Moncol, M. T. D. Cronin, M. Mazur, J. Telser, *Int. J. Biochem. Cell Biol.* **2007**, *39*, 44–84; d) L. M. Sayre, G. Perry, M. A. Smith, *Chem. Res. Toxicol.* **2008**, *21*, 172–188.
[2] M. J. Mate, G. Murshudov, J. Bravo, W. Melik-Adamyan, P. C. Loewen, I Fita, Ignacio in *Handbook of Metalloproteins*, vol. 1 (Ed.: A. Messerschmidt), John Wiley & Sons, Chichester, **2001**, pp. 486–502.
[3] A. J. Wu, J. E. Penner-Hahn, V. L. Pecoraro, *Chem. Rev.* **2004**, *104*, 903–938.
[4] a) S. V. Antonyuk, V. R. Melik-Adamyan, A. N. Popov, V. S. Lamzin, P. D. Hempstead, P. M. Harrison, P. J. Artymyuk, V. V. Barynin, *Crystallogr. Rep.* **2000**, *45*, 105–116; b) V. V. Barynin, M. M. Whittaker, S. V. Antonyuk, V. S. Lamzin, P. M. Harrison, P. J. Artymiuk, J. W. Whittaker, *Structure* **2001**, *9*, 725–738.
[5] S. Signorella, C. Hureau, *Coord. Chem. Rev.* **2012**, *256*, 1229–1245.
[6] a) B. J. Day, *Drug Discovery Today* **2004**, *9*, 557–566; b) B. J. Day, *Biochem. Pharmacol.* **2009**, *77*, 285–296.
[7] a) B. J. Day, I. Fridovich, J. D. Crapo, *Arch. Biochem. Biophys.* **1997**, *347*, 256–262; b) P. R. Castello, D. A. Dreschel, B. J. Day, M. Patel, *J. Pharm. Exp. Ther.* **2008**, *324*, 970–976.
[8] S. R. Doctrow, K. Huffman, C. B. Marcus, G. Tocco, E. Malfroy, C. A. Adinolfi, H. Kruk, N. Lazarowych, J. Mascarenhas, B. Malfroy, *J. Med. Chem.* **2002**, *45*, 4549–4558.
[9] B. Albela, R. Carina, C. Policar, S. Poussereau, J. Cano, J. Guilhem, L. Tchertanov, G. Blondin, M. Delroisse, J.-J. Girerd, *Inorg. Chem.* **2005**, *44*, 6959–6966.
[10] The complex has also been structurally characterized as the acetonitrile solvate after anion metathesis with $TlPF_6$ in MeCN, see Supporting Information.
[11] See Supporting Information for further details.
[12] W. A. Gunderson, A. I. Zatsman, J. P. Emerson, E. R. Farquhar, L. Que Jr., J. D. Lipscomb, M. P. Hendrich, *J. Am. Chem. Soc.* **2008**, *130*, 14465–14467.
[13] More comprehensive information on the kinetic parameters of mono- and dinuclear manganese catalase mimics can be found in ref.[5]
[14] Negligible oxygen evolution in the presence of $Mn(H_2O)_6^{2+}$ is observed under the same conditions.
[15] Given that we do not have full deuteration of the solvent or H_2O_2 as well as the multiple proton-dependent steps in the proposed mechanism, it is very difficult to interpret this value.
[16] R. G. Wilkins, *Kinetics and Mechanism of Reactions of Transition Metal Complexes*, 2nd ed., VCH, Weinheim, **1991**.
[17] J. Kaizer, B. Kripli, G. Speier, L. Párkányi, *Polyhedron* **2009**, *28*, 933–936.
[18] J. Kaizer, T. Csay, P. Kővári, G. Speier, L. Párkányi, *J. Mol. Catal. A* **2008**, *280*, 203–209.
[19] J. S. Pap, B. Kripli, I. Bors, D. Bogáth, M. Giorgi, J. Kaizer, G. Speier, *J. Inorg. Biochem.* **2012**, *117*, 60–70.
[20] R. Li, J. Tian, H. Liu, S. Yan-Shiping, S. Shouwu, J. Zhang, *Transition Met. Chem.* **2011**, *36*, 811–817.
[21] A. Mahammed, Z. Gross, *Chem. Commun.* **2010**, *46*, 7040–7042.

[22] a) A. Y. Satoh, J. E. Trosko, S. J. Masten, *Environ. Sci. Technol.* **2007**, *41*, 2881–2887; b) K. Kishore, S. N. Guha, J. Mahadevan, P. N. Moorthy, J. P. Mittal, *Radiat. Phys. Chem.* **1989**, *34*, 721–727.
[23] red-CLA = (2-{4-[4-(3,7-dihydro-2-methyl-3-oxoimidazo[1,2-*a*]-pyrazin-6-yl)phenoxy]butyramido}ethylamino)sulforhodamine 101.
[24] A. Godrant, A. L. Rose, G. Sarthou, T. D. White, *Limnol. Oceanogr. Methods* **2009**, *7*, 682–692.
[25] a) S. A. Mizra, B. Bocquet, C. Robyr, S. Thomi, A. F. Williams, *Inorg. Chem.* **1996**, *35*, 1332–1337; b) A. G. DiPasquale, J. M. Mayer, *J. Am. Chem. Soc.* **2008**, *130*, 1812–1813.
[26] K. Chen, M. Costas, J. Kim, A. K. Tipton, L. Que Jr., *J. Am. Chem. Soc.* **2002**, *124*, 3026–3035.
[27] a) Y. G. Abashkin, S. K. Burt, *J. Phys. Chem. B* **2004**, *108*, 2708–2711; b) Y. G. Abashkin, S. K. Burt, *Inorg. Chem.* **2005**, *44*, 1425–1432; c) S.-Y. Liu, J. D. Soper, J. Y. Yang, E. V. Rybak-Akimova, D. G. Nocera, *Inorg. Chem.* **2006**, *45*, 7572–7574.
[28] G. Yin, *Acc. Chem. Res.* **2013**, DOI: 10.1021/ar300208z.
[29] G. Yin, J. M. McCormick, M. Buchalova, A. M. Danby, K. Rodgers, V. W. Day, K. Smith, C. M. Perkins, D. Kitko, J. D. Carter, W. M. Scheper, D. H. Busch, *Inorg. Chem.* **2006**, *45*, 8052–8061.
[30] a) G. Yin, M. Buchalova, A. M. Danby, C. M. Perkins, D. Kitko, J. D. Carter, W. M. Scheper, D. H. Busch, *J. Am. Chem. Soc.* **2005**, *127*, 17170–17171; b) G. Yin, M. Buchalova, A. M. Danby, C. M. Perkins, D. Kitko, J. D. Carter, W. M. Scheper, D. H. Busch, *Inorg. Chem.* **2006**, *45*, 3467–3474.
[31] A. Xu, H. Xiong, G. Yin, *J. Phys. Chem. A* **2009**, *113*, 12243–12248.
[32] A. Haras, T. Ziegler, *Can. J. Chem.* **2009**, *87*, 33–38.
[33] For $[Me_2EBC]MnCl_2$: $E_{1/2}$ = 0.466 V (Mn^{II}/Mn^{III}), 1.232 V (Mn^{III}/Mn^{IV}). For $[(Py_2NMe_2)MnCl_2]$: $E_{1/2}$ = 0.496 V (Mn^{II}/Mn^{III}), 1.526 V (Mn^{III}/Mn^{IV}). All potentials are referenced to SCE in NBu_4PF_6/MeCN. See ref.[9,34]
[34] T. J. Hubin, J. M. McCormick, S. R. Collinson, M. Buchalova, C. M. Perkins, N. W. Alcock, P. K. Kahol, A. Raghunathan, D. H. Busch, *J. Am. Chem. Soc.* **2000**, *122*, 2512–2522.
[35] M. Delroisse, A. Rabion, F. Chardac, D. Tétard, J.-B. Verlhac, L. Fraisse, J.-L. Séris, *J. Chem. Soc., Chem. Commun.* **1995**, 949–950.
[36] P. A. Goodson, D. J. Hodgson, K. Michelsen, *Inorg. Chim. Acta* **1990**, *172*, 49–57.
[37] P. A. Goodson, D. J. Hodgson, J. Glerup, K. Michelsen, H. Weihe, *Inorg. Chim. Acta* **1992**, *197*, 141–147.
[38] W. Baker, K. M. Buggle, J. F. W. McOmie, D. A. M. Watkins, *J. Chem. Soc.* **1958**, 3594–3603.
[39] M. V. Lakshmikantham, Y. A. Jackson, M. P. Cava, *J. Org. Chem.* **1988**, *53*, 3529–3532.
[40] M. V. Baker, L. D. Field, T. W. Hambley, *Inorg. Chem.* **1988**, *27*, 2872–2876.
[41] The rate of hydrogen exchange between H_2O and H_2O_2 is 1.6×10^7 $M^{-1}s^{-1}$ under acidic conditions: M. Anbar, A. Loewenstein, S. Meiboom, *J. Am. Chem. Soc.* **1958**, *80*, 2630–2634.

Received: February 5, 2013
Published Online: May 31, 2013

